

in a time less than 10 nsec and that the alignment which remained persisted for over 750 nsec. This suggests that perhaps about $\frac{1}{3}$ of the ions come to rest in interstitial sites where a large quadrupole interaction can destroy the alignment in less than 10 nsec, while the remaining ions find lattice sites of the cubic Cu lattice where the alignment is maintained. Since the observed alignment for implanted nuclei of psec lifetimes reach the theoretical estimate in Cu,¹² it is suggested that the relaxa-

tion time of the quadrupole interaction at interstitial positions in Cu is $10 \text{ psec} < \tau_r < 10 \text{ nsec}$ with, of course, some dependence on the magnitude of the quadrupole moment. The fraction of implanted recoils which find lattice sites undoubtedly depends on the kind of recoils and the type of backing material. Sprouse *et al.*,¹³ for example, find from Mössbauer experiments that larger fractions of implanted Fe⁵⁷ nuclei reach lattice sites in several different backings in less than 100 nsec.

¹² R. Kalish, L. Grodzins, R. R. Borchers, J. D. Bronson, and B. Herskind, Phys. Rev. **161**, 1196 (1967).

¹³ G. D. Sprouse, G. M. Kalvius, and S. S. Hanna, Phys. Rev. Letters **18**, 1041 (1967).

Nuclear Structure of Na²². IV. Gamma-Ray Correlation Measurements*

E. K. WARBURTON, A. R. POLETTI,[†] AND J. W. OLNES

Brookhaven National Laboratory, Upton, New York

(Received 1 December 1967)

γ - γ angular correlations have been measured relative to the α beam in the $F^{19}(\alpha, n\gamma\gamma)Na^{22}$ reaction using NaI(Tl) γ -ray detectors. An ancillary determination of γ branching ratios for Na²² states of interest was made through γ - γ coincidence measurements utilizing Ge(Li) and NaI(Tl) detector combinations. From these measurements and previous information it was determined that the Na²² 1.95-, 2.97-, and 3.06-MeV levels have $J=2$, 3, and 2, respectively. The quadrupole-dipole amplitude ratios of the $1.95 \rightarrow 0.58$, $2.97 \rightarrow 1.95$, and $3.06 \rightarrow 1.95$ transitions were determined to be $+(0.04 \pm 0.06)$, $+(0.017 \pm 0.034)$, and $-(0.05 \pm 0.15)$, respectively; i.e., the results are consistent in each case with pure dipole radiation. From measurements of the angular correlation of the Na²² $1.528 \rightarrow 0.891 \rightarrow 0$ γ -ray cascade, it was determined that the two members of this $5^+ \rightarrow 4^+ \rightarrow 3^+$ cascade have $E2/M1$ amplitude ratios of $-(2.00 \pm 0.15)$ and $-(3.08 \pm 0.32)$, respectively. From these mixing ratios and previously determined branching ratios and lifetimes for the Na²² 1.528- and 0.891-MeV levels the $E2$ strengths of the $1.528 \rightarrow 0.891$ and $0.891 \rightarrow 0$ transitions are 20.7 ± 7.0 and 29.5 ± 4.5 Weisskopf units, respectively. These and other properties of Na²² are in accord with a rotational-model interpretation of this nucleus.

I. INTRODUCTION

IN this report we present further results in a continuing experimental investigation of the nucleus Na²². Information available on the quantum numbers of the first 18 levels of Na²² and the first 3 levels of Ne²² is shown in Fig. 1. The figure is taken mainly from previous reports¹⁻⁴ from this laboratory on the levels of Na²². Those levels for which spin information was provided by the present work are marked by an asterisk.

Evidence for a collective-model description of the Na²² level structure has been discussed previously. It seems likely the Na²² ground state, 0.891-, and 1.528-MeV levels are members of a $K=3$ rotational band. Particu-

lar interest is therefore attached to the determination of the $E2/M1$ amplitude ratios for the $1.528 \rightarrow 0.891$ and $0.891 \rightarrow 0$ transitions. The branching ratios and the lifetimes are known for both the 1.528- and 0.891-MeV states.¹⁻⁷ Thus, a determination of these $E2/M1$ ratios would uniquely determine the $E2$ and $M1$ strengths of these two transitions which together with the $E2$ strength of the $1.528 \rightarrow 0$ transition would provide a further test of the rotational-model interpretation of these 3 states. With respect to this latter interest, it is clear that additional information on spin-parity assignments for the higher-lying Na²² levels is also most desirable.

The purpose of the present experimental investigation was therefore twofold: (1) to determine the $E2/M1$ amplitude ratios for the Na²² $1.528 \rightarrow 0.891$ and $0.891 \rightarrow 0$ transitions; (2) to determine the spins of the 1.95-, 2.97-, and 3.06-MeV levels of Na²². The method we

* Work performed under the auspices of the U. S. Atomic Energy Commission.

[†] Present address: Lockheed Missiles and Space Corporation, Palo Alto, Calif.

¹ E. K. Warburton, J. W. Olnes, and A. R. Poletti, Phys. Rev. **160**, 938 (1967).

² A. R. Poletti, E. K. Warburton, J. W. Olnes, and S. Hecht, Phys. Rev. **162**, 1040 (1967).

³ A. R. Poletti, E. K. Warburton, and J. W. Olnes, Phys. Rev. **164**, 1479 (1967).

⁴ A. Gallmann, G. Frick, E. K. Warburton, D. E. Alburger, and S. Hecht, Phys. Rev. **163**, 1190 (1967).

⁵ J. G. Pronko, C. Rolfs, and H. J. Maier, Phys. Rev. **167**, 1066 (1968).

⁶ A. E. Blaugrund, A. Fisher, and A. Schwartzschild, Nucl. Phys. **A107**, 411 (1968).

⁷ R. W. Kavanagh, Bull. Am. Phys. Soc. **12**, 913 (1967).

have used was to measure the angular correlations between two γ rays in each of the Na^{22} $3.06 \rightarrow 1.95 \rightarrow 0.58$, $2.97 \rightarrow 1.95 \rightarrow 0.58$, and $1.53 \rightarrow 0.89 \rightarrow 0$ cascades following population of the initial level of the cascade via the $\text{F}^{19}(\alpha, n)\text{Na}^{22}$ reaction. Since this reaction results in alignment of the initial level the correlation is a triple one. We use the method of analysis initiated by Warburton and Rose⁸ and developed by Litherland and Ferguson⁹ (method I).

The γ - γ angular correlations were measured with NaI(Tl) detectors. The experimental resolution was clearly not good enough to resolve the γ rays arising from the various possible decay modes of these Na^{22} levels; e.g., γ rays from the $3.06 \rightarrow 1.95$ and $3.06 \rightarrow 1.98$ transitions (see Fig. 1). Thus a proper interpretation of the γ - γ angular correlations required that the γ -branching of the 1.95-, 2.97-, and 3.06-MeV levels be determined by other means as described in Sec. II. The γ - γ angular correlation measurements are described in Sec. III, and the results of these measurements are discussed in Sec. IV.

TABLE I. γ -ray branching ratios for the Na^{22} levels studied in the present work.

E_i (MeV)	E_f (MeV)	E_γ (keV)	Branching ratio (%)
0.891	0	890.9	100
	0.583	307.8	<0.5
	0.657	233.9	<0.5
1.528	0	1528.1	95.5 \pm 1.2
	0.583	945.0	<0.5
	0.657	871.1	<0.5
	0.891	637.2	4.5 \pm 1.2
1.952	0	1951.8	<2
	0.583	1368.8	100
	0.657	1294.8	<3
	0.891	1060.9	<0.5
	1.528	423.7	<0.5
2.969	0	2968.6	<1
	0.583	2385.6	<1
	0.657	2311.6	<1
	0.891	2077.7	<1
	1.528	1440.5	<0.5
	1.937	1031.7	<0.7
	1.952	1016.8	100
	1.984	985.1	<4
	2.211	757.2	<2
3.059	2.572	397.1	<2
	0	3059.4	<1
	0.583	2476.4	3 \pm 1
	0.657	2402.4	<1
	0.891	2168.5	<2
	1.528	1531.3	<3
	1.937	1122.5	<2
	1.952	1107.6	97 \pm 1
	1.984	1075.9	<2
	2.211	848.0	<4
	2.572	487.9	<3

⁸ E. K. Warburton and H. J. Rose, Phys. Rev. **109**, 1199 (1958).

⁹ A. E. Litherland and A. J. Ferguson, Can. J. Phys. **39**, 788 (1961); A. J. Ferguson, *Angular Correlation Methods in Gamma-Ray Spectroscopy* (North-Holland Publishing Co., Amsterdam, 1965).

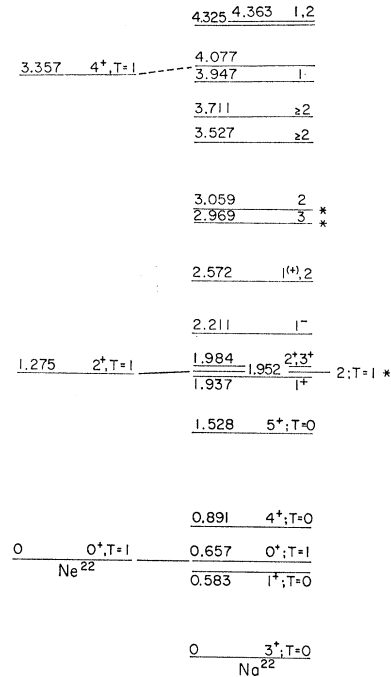


FIG. 1. The low-lying levels of Na^{22} and Ne^{22} . The figure is from Ref. 2 with some additions. The sources of the data are cited in Refs. 1 and 2. Asterisks denote those Na^{22} levels for which the present work results in new information concerning spin assignments.

II. γ -RAY BRANCHING RATIOS

The γ -ray branching ratios of the Na^{22} levels of interest are listed in Table I. These results are taken from Ref. 1 but incorporate sharper upper limits on the relative intensities of the $2.97 \rightarrow 1.53$, $2.97 \rightarrow 1.98$, and $3.06 \rightarrow 1.98$ transitions, which were previously¹ reported to be <2, <6, and <16%, respectively. The limits listed in Table I for these three transitions were determined from Ge(Li)-NaI(Tl) γ -ray coincidence measurements which we shall now describe.

Levels of Na^{22} were populated via the $\text{F}^{19}(\alpha, n)\text{Na}^{22}$ reaction ($Q = -1.949$ MeV), using a $250\text{-}\mu\text{g}/\text{cm}^2$ CaF_2 target on a Ni backing and a 7.2-MeV doubly ionized α beam from the BNL 3.5-MV electrostatic generator. The γ rays from the above reaction were detected by a $3 \times 3\text{-in.}$ NaI(Tl) crystal and by a 20-cc Ge(Li) detector. Both detectors were ~ 2 cm from the target. Time-coincident pulses, as determined by an external circuit of $2\tau = \sim 100$ nsec, were displayed in a $32(\text{NaI}) \times 512(\text{Ge})$ mode of a TMC 2¹⁴-channel two-parameter analyzer. The analyzer was set to record NaI(Tl) pulses in the range $0.9 \leq E_\gamma \leq 1.8$ MeV and Ge(Li) pulses in the range $0.75 \leq E_\gamma \leq 1.5$ MeV. The beam current was ~ 30 nA and the reals/random ratio was $\sim 25/1$. Two separate two-parameter spectra were recorded: one with both detectors at 90° to the beam and opposite each other and the other with the Ge(Li) detector at 0° to the beam. The collection time for each of the two spectra was ~ 20 h.

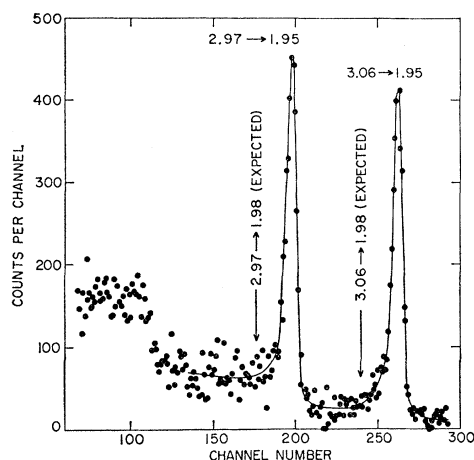


FIG. 2. Partial spectrum of γ rays from the $F^{19}(\alpha, n)Na^{22}$ reaction observed with a 20-cc Ge(Li) detector in coincidence with ~ 1.4 -MeV γ rays from a 3×3 -in. NaI(Tl) detector. The digital gate on the NaI(Tl) detector encompassed completely the region of the 1.40-MeV full-energy peak of the $1.98 \rightarrow 0.58$ transition, and also $\sim 66\%$ of the full-energy peak of the (unresolved) 1.37-MeV $1.95 \rightarrow 0.58$ transition. The data were acquired at a bombarding energy $E_\alpha = 7.2$ MeV to investigate the relative branching of the 2.97- and 3.06-MeV levels to the 1.95- and 1.98-MeV levels. The Ge(Li) and NaI(Tl) detectors were set at angles $\theta_\gamma = 0^\circ$ and 90° , respectively. The previously reported $2.97 \rightarrow 1.95$ and $3.06 \rightarrow 1.95$ transitions, seen in coincidence with 1.37-MeV γ rays, are clearly evident. From the absence of peaks corresponding to possible $2.97 \rightarrow 1.98$ and $3.06 \rightarrow 1.98$ transitions, which would be coincident with 1.40-MeV γ rays, upper limits on the relative intensity of these transitions are derived as given in the text.

Each spectrum showed clearly evidence for coincidence between γ rays of energy 1017 and 1369 keV from the $2.97 \rightarrow 1.95 \rightarrow 0.58$ cascade, and of energy 1108 and 1369 keV from the $3.06 \rightarrow 1.95 \rightarrow 0.58$ cascade. No evidence was found for γ rays from the $3.06 \rightarrow 1.98$ or $2.97 \rightarrow 1.98$ transitions which would appear in coincidence with 1401-keV γ rays from the subsequent $1.98 \rightarrow 0.58$ decay. Figure 2 shows the Ge(Li) spectrum coincident with the pulse-height region [in the NaI(Tl) detector] corresponding to a 1401-keV photopeak. Since the digital gate set on the region of the 1401-keV photopeak in the NaI(Tl) detector also encompassed a portion of the 1369-keV photopeak (unresolved in singles) Fig. 2 also exhibits the 1108- and 1017-keV peaks from the $3.06 \rightarrow 1.95 \rightarrow 0.58$ and $2.97 \rightarrow 1.95 \rightarrow 0.58$ cascades, respectively. The upper limits listed in Table I for the relative intensities of the $2.97 \rightarrow 1.98$ and $3.06 \rightarrow 1.98$ branches (and also the $2.97 \rightarrow 1.53$ branch) result from a quantitative analysis of these two-parameter spectra. By comparing the data obtained with the Ge(Li) detector at 0° and also at 90° it was determined that the effects of possible angular correlations on these limits are minimal.

In summary, the upper limits listed in Table I for the possible decay (unobserved) of the 3-MeV doublet to the 1.94- and 1.98-MeV levels and the possible decay of the 1.95-MeV level to the 0.66-MeV level (also unobserved) are small enough so that the maximum possi-

ble admixtures of these transitions in the $2.97 \rightarrow 1.95 \rightarrow 0.58$ and $3.06 \rightarrow 1.95 \rightarrow 0.58$ cascades would have only a negligible effect on the angular correlation analysis described in the next section.

III. γ - γ CORRELATIONS

A. Experimental Procedure

Again, the $F^{19}(\alpha, n)Na^{22}$ reaction was employed using a $250\text{-}\mu\text{g}/\text{cm}^2$ CaF_2 target evaporated onto an 0.1-mil Ni backing. For the study of the Na^{22} $1.528 \rightarrow 0.891 \rightarrow 0$ cascade, a 4.9-MeV α beam of 40-nA intensity was used. At this bombarding energy no evidence was found for population of any Na^{22} levels above the 1.53-MeV level. The 3-MeV doublet levels of Na^{22} at 3.06- and 2.97-MeV were studied with a 7.2-MeV α beam of ~ 50 nA. At this energy, the same as used in the Ge(Li)-NaI(Tl) coincidence measurements, no evidence was observed for population of Na^{22} levels with excitation energies greater than 3.1 MeV.

Two 3×3 -in. NaI(Tl) detectors were used for these correlation measurements. The first was fixed in the horizontal plane at 90° to the beam and 10 cm from the target. A second detector, mounted on a goniometer at a distance of 10 cm from the target, was moved about the edges of the *forward, upper* octant¹⁰ on the *other* side of the target from the fixed 90° crystal. In a spherical coordinate system centered at the target with the beam axis designated as the z axis, we define our coordinates such that the fixed 90° crystal is at $\theta = 90^\circ$, $\phi = 0^\circ$. Then as the variable crystal is moved about the octant starting at 0° to the beam it traces out the following 3 arcs: (1) $\phi = 180^\circ$, $\theta = 0^\circ$ to 90° , (2) $\phi = 180^\circ$ to 90° , $\theta = 90^\circ$; and (3) $\phi = 90^\circ$, $\theta = 90^\circ$ to 0° . The normal to the target face was set in the direction $\theta = 135^\circ$, $\phi = 315^\circ$, i.e., at 180° to the center of the octant; thus absorption in the target backing (10 mil of Ta) was minimized.

For each of the three paths (arcs) along the edges of the octant, data were recorded in random order for five values of the variable angle, e.g., $\theta = 0^\circ$, 30° , 45° , 60° , and 90° for $\phi = 180^\circ$. Each measurement consisted of a 128×128 two-dimensional spectra of time-coincident pulses from the fixed ($\theta, \phi = 90^\circ, 0^\circ$) crystal and the variable crystal. In all, 15 spectra were recorded for a complete traversal of the octant. These included two spectra taken at each of the three corners of the octant. This procedure was then repeated so that 30 spectra were recorded for both $E_\alpha = 4.9$ MeV and $E_\alpha = 7.2$ MeV. In all, the measurements reported here took about 7 days of continuous operation (~ 2.5 h per spectrum).

Conventional fast-slow coincidence circuits were used to define time coincident events. The resolving time was ~ 70 nsec and the reals/random ratio varied from ~ 12 to ~ 20 . The gains of the two NaI(Tl) detectors were carefully adjusted to be equal, and were stabilized throughout these measurements by Cosmic Radiation

¹⁰ C. Broude and H. E. Gove, Ann. Phys. (N. Y.) **23**, 71 (1963).

Inc. "Spectrostats" operating on the 0.583-MeV γ ray from the Na^{22} $0.583 \rightarrow 0$ transition. Thus the two axes of the 128×128 spectra displayed identical γ -ray spectra (aside from angular correlation effects). This considerably reduced the labor of analysis.

At both α energies the Ne^{22} 3.357-MeV level was strongly formed via the $\text{F}^{19}(\alpha, p)\text{Ne}^{22}$ reaction ($Q = 1.675$ MeV). The two-dimensional spectra were normalized to the coincidence rate of the Ne^{22} $3.357 \rightarrow 1.27 \rightarrow 0$ correlation recorded between the fixed ($\theta, \phi = 90^\circ, 0^\circ$) crystal and a (third) monitor crystal placed at $\theta = 135^\circ$. This rate was measured by a fast-slow coincidence circuit with pulse-height windows set on the full-energy peaks of the 1.27-MeV γ ray (fixed crystal) and the 2.08-MeV γ ray (monitor crystal). The ratio of this coincidence rate to the integrated beam charge was constant within experimental uncertainties ($< 2\%$) for each α energy.

B. Reduction of Data

$2.97 \rightarrow 1.95 \rightarrow 0.58$ and $3.06 \rightarrow 1.95 \rightarrow 0.58$ Cascades

Figure 3 illustrates some results of the two-parameter analysis and serves to exemplify the procedures used in the reduction of the correlation data. We are here interested in the angular correlation of 1.02- and 1.37-MeV γ rays from the $2.97 \rightarrow 1.95 \rightarrow 0.58 \rightarrow 0$ cascade and that of 1.11- and 1.37-MeV γ rays from the $3.06 \rightarrow 1.95 \rightarrow 0.58 \rightarrow 0$ cascade.

Figure 3(A) shows the γ spectrum measured by the fixed ($\theta, \phi = 90^\circ, 0^\circ$) detector in coincidence with a digital gate set on the 1.02- and 1.11-MeV peaks as seen in the moving ($\theta, \phi = \text{variable}$) detector. The 1.37-MeV γ ray, which arises as the second member of each cascade, is clearly evident, as is the 0.58-MeV γ ray from the subsequent de-excitation of the 0.583-MeV state. The intensity of the latter γ ray is weaker because the resolving time of the coincidence circuitry is shorter than the transition lifetime,¹¹ and hence the γ ray is detected in coincidence with markedly decreased efficiency. The 1.27-MeV γ ray is from the Ne^{22} $3.36 \rightarrow 1.27 \rightarrow 0$ cascade, and arises from coincidences with those Compton pulses from the 2.08-MeV γ ray which lie within the digital gate set on the 1.02- and 1.11-MeV peaks. The approximately flat background upon which the 1.37-MeV peak is superimposed arises mainly from Compton scattering of higher-energy γ rays.

In order to determine the spectrum of γ rays coincident with 1.37-MeV γ rays the following procedure was adopted. First, a spectrum designated Σ was constructed as the spectrum coincident with the indicated pulse-height region in Fig. 3(A). The background in this spectrum was estimated as the sum of the spectra coincident with regions B_1 and B_2 and was subtracted off to yield the corrected spectrum designated $\Sigma - B$. Resultant spectra ($\Sigma - B$) showing the 1.02- and 1.11-MeV γ rays coin-

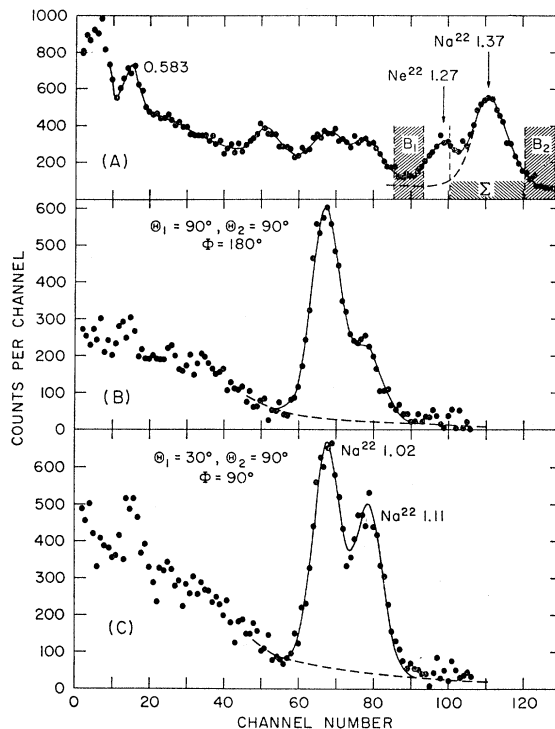


FIG. 3. Portions of two of the 30×128 -channel two-parameter NaI(Tl)-NaI(Tl) γ -ray spectra recorded following the bombardment of a CaF_2 target with 7.2-MeV α particles. In (A) is shown the NaI(Tl) spectrum in coincidence with the region of pulse height between channels 50 and 90 in the other NaI(Tl) crystal. As is seen from (B) and (C), this region encompasses the full-energy peaks of the 1.02-MeV $2.97 \rightarrow 1.95$ and 1.11-MeV $3.06 \rightarrow 1.95$ transitions. (Note that the gain of the two γ -ray detectors are equal.) Thus, in (A) we see the full-energy peaks of the 1.37- and 0.58-MeV γ rays which are in coincidence with both the 1.02- and 1.11-MeV γ rays as well as the full-energy peak of the Ne^{22} 1.27-MeV γ ray which is in coincidence with the background under the 1.02- and 1.11-MeV γ rays. In (B) and (C) are shown spectra, for two different geometrical arrangements of the detectors, in coincidence with the 1.37-MeV full-energy peak. In these spectra, designated $\Sigma - B$, the effects of the background underlying the 1.37-MeV peak have been largely removed, as indicated in (A). The dashed curves of (B) and (C) are the assumed backgrounds under the composite 1.02- and 1.11-MeV peaks and the solid curves are least-squares fits assuming two unresolved Gaussian peaks (see text).

cident with 1.37-MeV γ rays, are illustrated for two detection angles in Figs. 3(B) and 3(C). The intensities of the unresolved 1.02- and 1.11-MeV γ rays were determined by a computer analysis which fitted the ($\Sigma - B$) spectra as the sum of two Gaussian peaks superimposed on an (assumed) exponential background. The results are shown by the solid curves of Figs. 3(B) and 3(C). The background level, shown by the dashed curve, was fitted to the regions immediately above and below the peak region. The relative pulse heights of the two peaks were constrained to be consistent with their known energies¹ and their widths were constrained to be proportional to the square roots of their energies. The latter restriction ensures that the fitted peak widths shall be consistent with the previously determined characteristics of the detectors.

¹¹ A. W. Sunyar and P. Thieberger, Phys. Rev. **151**, 910 (1966).

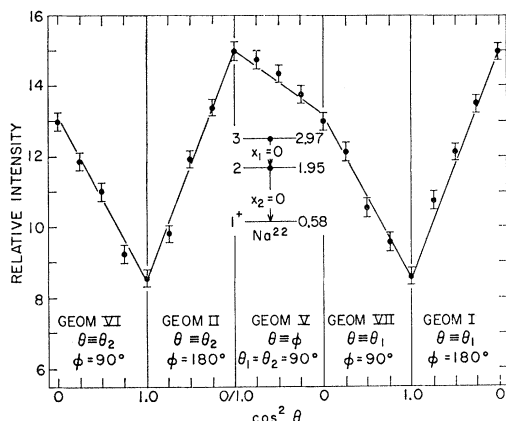


FIG. 4. Results of the γ - γ triple correlation measurement for the Na^{22} $2.97 \rightarrow 1.95 \rightarrow 0.58$ cascade. The experimental points are shown for the five indicated geometries. The geometries are explained in the text and in Ref. 9. The solid curve is the fit to these data for the spin values and mixing ratios indicated in the level scheme.

If we designate the first and second γ ray in a γ -ray cascade by γ_1 and γ_2 , respectively, and the angles at which they are detected by θ_1 , ϕ_1 , and θ_2 , ϕ_2 , then a given two-dimensional spectrum has γ_2 detected at θ_1 , ϕ_1 in coincidence with γ_1 detected at θ_2 , ϕ_2 as well as γ_2 detected at θ_2 , ϕ_2 and γ_1 detected at θ_1 , ϕ_1 . Thus 60 spectra similar to that in Figs. 3(B) and 3(C) were generated and analyzed. For each, the number of counts in the full-energy peaks of the 1.02- and 1.11-MeV γ rays were determined. These were then normalized to the Ne^{22} $3.357 \rightarrow 1.27 \rightarrow 0$ coincidence rate observed between the fixed and monitor crystals.

Because the initial Na^{22} level is aligned by the reaction used to form it, the coincidence rate with γ_1 at θ_1 , ϕ_1 ; γ_2 at θ_2 , ϕ_2 is not necessarily the same as that for γ_2 at θ_1 , ϕ_1 ; γ_1 at θ_2 , ϕ_2 . The relative counting rates for the two detection processes, as obtained from the procedures of analysis outlined above, may have been influenced

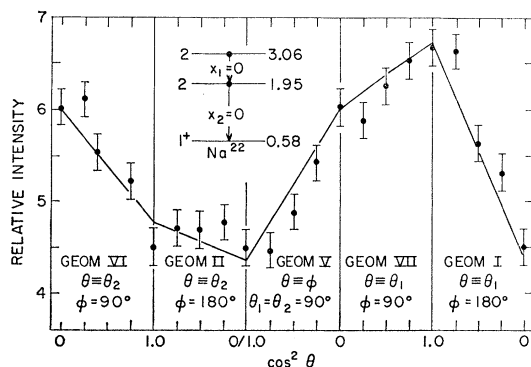


FIG. 5. Results of the γ - γ triple correlation measurement for the Na^{22} $3.06 \rightarrow 1.95 \rightarrow 0.58$ cascade. The experimental points are shown for the five indicated geometries. The geometries are explained in the text and in Ref. 9. The solid curve is the fit to these data for the spin values and mixing ratios indicated in the level scheme.

also by the slightly different gain, resolution, and efficiency of the two detectors. (Note, however, that the latter effect is possible only if the two detection efficiencies have different energy dependencies.) For the case $\theta_1 = \theta_2 = 90^\circ$, however, the angular correlation is a function of $\phi_1 - \phi_2 = \phi$, only, and is independent of whether $\gamma_1(\gamma_2)$ is detected at $\phi_2(\phi_1)$ or $\phi_1(\phi_2)$. Thus the 20 spectra taken along the octant edge $\theta = 90^\circ$ (geometry V of Litherland and Ferguson)⁹ were used to determine a normalization constant which was subsequently applied to the data for the remaining four geometries.

The angular correlations obtained for the $2.97 \rightarrow 1.95 \rightarrow 0.58$ and $3.06 \rightarrow 1.95 \rightarrow 0.58$ cascades are shown in Figs. 4 and 5, respectively. The fits to these correlations will be described in Sec. III C. In these two figures

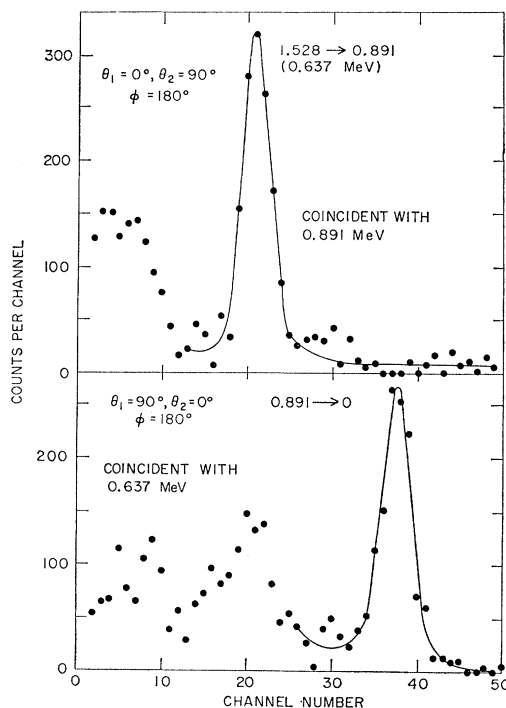


FIG. 6. Portions of one of the 30 128×128 -channel two-parameter $\text{NaI}(\text{Tl})$ - $\text{NaI}(\text{Tl})$ γ -ray spectra recorded following the bombardment of a CaF_2 target with 4.9-MeV α particles. The Na^{22} $1.528 \rightarrow 0.891 \rightarrow 0$ cascade is being investigated. Each of the two partial spectra shows one of the two γ rays in this cascade in coincidence with the other. The procedure used in obtaining these spectra is identical to that exemplified in Fig. 3.

the angular correlations are defined by the nomenclature of Litherland and Ferguson.⁹ The polar angle ϕ_i , $i=1$ or 2, designates whether γ_1 or γ_2 is detected in the crystal moving about the octant, and $\phi = \phi_1 - \phi_2$.

$1.528 \rightarrow 0.891 \rightarrow 0$ Cascade

The analysis of the measurements made at $E_\alpha = 4.9$ MeV proceeded in a similar fashion to that just described with some small differences. The dispersion of the two-parameter analysis was decreased so that the

two-dimensional spectra would include also the 2.08-MeV γ ray from Ne^{22} . This was done so that the Ne^{22} $3.36 \rightarrow 1.27 \rightarrow 0$ angular correlation could be obtained simultaneously as a check on the procedure and on possible systematic errors.

The spectra in coincidence with the full-energy peaks of the 0.637- and 0.891-MeV γ rays from the $1.528 \rightarrow 0.891 \rightarrow 0$ cascade were extracted from the two-dimensional data in a fashion similar to that described for the analysis of the 3-MeV doublet levels. Some results from one of the two-dimensional spectra are shown in Fig. 6. In this same case, however, spectra in coincidence with both γ_1 and γ_2 were displayed for each crystal so that four spectra were generated from each two-dimensional spectra, rather than two as in the case of the study of the 3-MeV doublet. Each was graphically analyzed to obtain the number of counts in the full-energy peak of the γ ray displayed. Then the two results for the same values of θ_1 and ϕ_1 were averaged. This procedure was followed in order to reduce systematic errors arising from the "spectrum stripping." These errors were, in this case, the dominant ones since the $1.528 \rightarrow 0.891$ transition has a branching ratio¹ of only $(4.5 \pm 1.2)\%$. In other respects the data reduction was identical to that already described. The angular correlation obtained for the $1.528 \rightarrow 0.891 \rightarrow 0$ cascade is shown in Fig. 7.

Ne^{22} $3.36 \rightarrow 1.27 \rightarrow 0$ Cascade

The angular correlation for this cascade was obtained from the same data and in an identical fashion as the Na^{22} $1.528 \rightarrow 0.891 \rightarrow 0$ cascade. In this case, however, the "spectrum stripping" procedure had negligible uncertainty associated with it since there were no coincident γ rays observed with $E_\gamma > 1$ MeV except those of 1.27 and 2.08 MeV. The angular correlation for this cascade is shown in Fig. 8. The solid curve is a least-squares fit to this data assuming a $4^+ \rightarrow 2^+ \rightarrow 0^+$ sequence with the $4^+ \rightarrow 2^+$ transition pure E2 as demanded by earlier work.^{12,13} The excellent agreement between the theoretical and experimental correlations, as displayed in Fig. 8, confirms that possible misalignments are less than the figure 2%, which was the estimated accuracy with which the purely geometric alignment of the correlation apparatus was carried out. The data of Fig. 8 were subsequently used to determine a small ($< 2\%$) alignment correction for the Na^{22} data.

More importantly, the results of Fig. 8 provide a gauge for the estimation of possible systematic errors, including both residual misalignment errors and errors in the data-monitor normalization. From the Ne^{22} data (Fig. 8) a small constant (in θ , ϕ) uncertainty was determined which, when added to the statistical uncertainty of each point, was such as to make the external

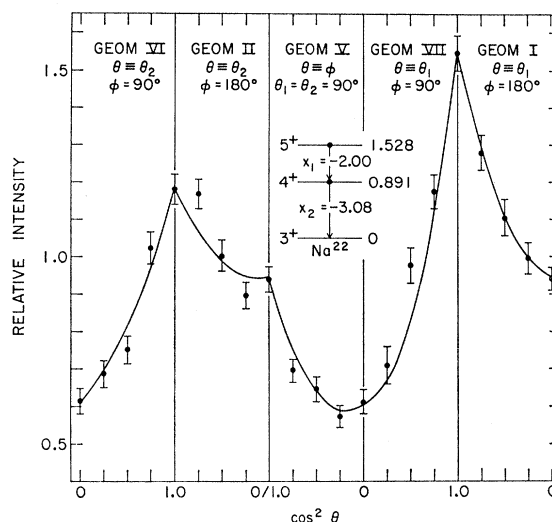


Fig. 7. Results of the γ - γ triple correlation measurement for the Na^{22} $1.528 \rightarrow 0.891 \rightarrow 0$ cascade. The experimental points are shown for the five indicated geometries. The geometries are explained in the text and in Ref. 9. The solid curve is the fit to these data for the spin values and mixing ratios indicated in the level scheme.

and internal errors equal, i.e., makes χ^2 equal to the degrees of freedom. Under the assumption that this was a valid estimate of the systematic error, the constant uncertainty so derived was added also to the statistical uncertainties for the Na^{22} correlation data.

C. Analysis

General

The analysis of the triple correlations was carried out with the aid of a computer program which fitted the experimental data with a theoretical correlation by the method of linear least-squares.¹⁰ The fits were made for discrete values of the quadrupole/dipole amplitude

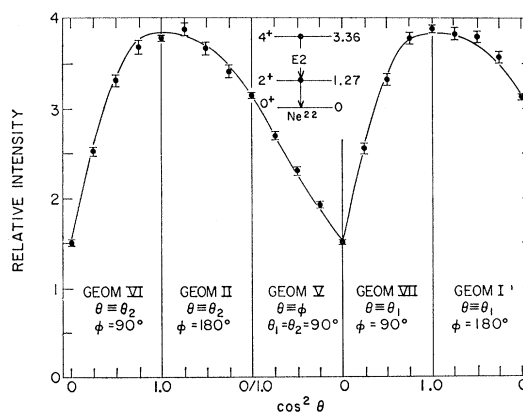


Fig. 8. Results of the γ - γ triple correlation measurements for the Ne^{22} $3.36 \rightarrow 1.27 \rightarrow 0$ cascade. The experimental points are shown for the five indicated geometries. The geometries are explained in the text and in Ref. 9. The solid curve is the fit to the data for the spin values indicated in the level scheme and assuming both transitions are pure quadrupole.

¹² D. Pelte, B. Povh, and W. Scholz, Nucl. Phys. **52**, 333 (1964); S. Buhl, D. Pelte, and B. Povh, *ibid.* **A91**, 319 (1967).

¹³ C. Broude and M. A. Eswaran, Can. J. Phys. **42**, 1300 (1964); M. A. Eswaran and C. Broude, *ibid.* **42**, 1311 (1964).

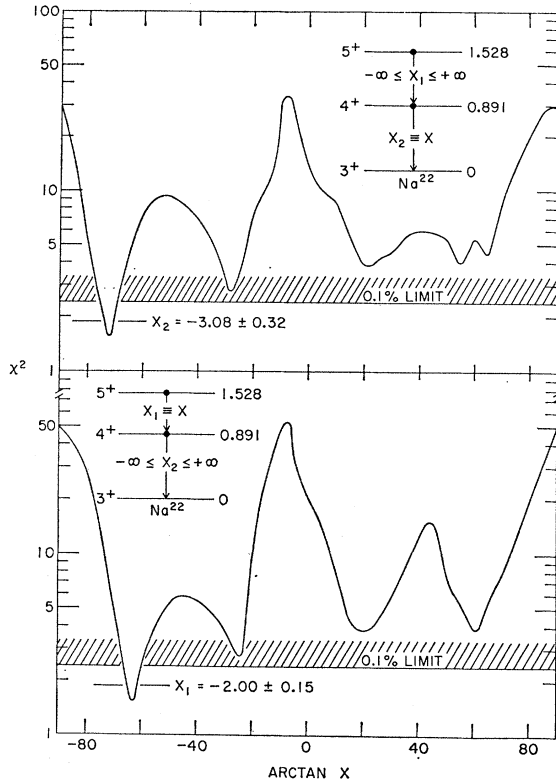


FIG. 9. χ^2 -versus- $\arctan x$ curves for the Na^{22} 1.528 \rightarrow 0.891 \rightarrow 0 cascade. The least-squares fit was to the data of Fig. 7. Each of the two curves shows χ^2 versus the $E2/M1$ mixing ratio of the indicated transition with no constraint of the mixing ratio of the other transition. The only acceptable solution, i.e., χ^2 less than the 0.1% limit, has $x_1 = -(2.00 \pm 0.15)$ and $x_2 = -(3.08 \pm 0.32)$.

ratios of the two transitions with the parameters describing the relative population of the magnetic substates of the initial level as variables. The output consists of the best values of these population parameters $P(m)$ and the value of χ^2 —which represents the goodness-of-fit, and has an expectation value of unity since

TABLE II. Restrictions on quadrupole/dipole mixing ratios of the first (x_1) and second (x_2) cascades of the Na^{22} 2.97 \rightarrow 1.95 \rightarrow 0.58 and 3.06 \rightarrow 1.95 \rightarrow 0.58 cascades and on the possible spin combinations of the three levels in question. The restrictions result from lifetime measurements^a and $\text{Ne}^{20}(\text{He}^3, p)\text{Na}^{22}$ angular correlation measurements.^b The restrictions obtained for the mixing ratios of the 3.06 \rightarrow 1.95, 2.97 \rightarrow 1.95, and 1.95 \rightarrow 0.58 transitions from the two cascades considered are interdependent.

J_1	J_2	Mixing ratio restrictions	
2.97 \rightarrow 1.95 \rightarrow 0.58			
1	2	$-0.30 < x_1 < -0.19$;	$-0.08 < x_2 < +0.56$
2	1	$-0.12 < x_1 < +0.30$;	$+0.34 < x_2 < +0.56$
3	2	$-0.07 < x_1 < +0.07$;	$-0.14 < x_2 < +0.14$
3.06 \rightarrow 1.95 \rightarrow 0.58			
1	1	$-0.32 < x_1 < 0.00$;	$+0.34 < x_2 < +0.56$
1	2	$-0.32 < x_1 < -0.19$;	$-0.14 < x_2 < -0.02$
2	2	$-0.18 < x_1 < +0.21$;	$-0.14 < x_2 < +0.56$
3	2	$-0.30 < x_1 < -0.24$;	$-0.14 < x_2 < -0.08$

^a Reference 1.

^b Reference 2.

it is normalized to the degrees of freedom. This procedure was repeated for discrete values of x_1 and x_2 —the quadrupole/dipole amplitude ratios of γ_1 and γ_2 , respectively. In general, this was done for all the allowed values of the spins of the three levels involved. Thus, for each spin combination, a contour map of χ^2 versus x_1 and x_2 was generated and inspected to obtain information concerning x_1 and x_2 and the spins of the three levels involved.

For the Ne^{22} 3.36 \rightarrow 1.27 \rightarrow 0 data of Fig. 8 both transitions are pure $E2$ and only one spin combination and unique values for x_1 and x_2 were used. This fit of Fig. 8 corresponds to the following values for the magnetic substate population parameters:

$$\begin{aligned} P(0) &= 0.345 \pm 0.007, \\ P(1) &= 0.242 \pm 0.005, \\ P(2) &= 0.083 \pm 0.006, \\ P(3) &= 0.002 \pm 0.003, \\ P(4) &= 0.0. \end{aligned}$$

These have been normalized so that

$$\sum_m P(m) = 1,$$

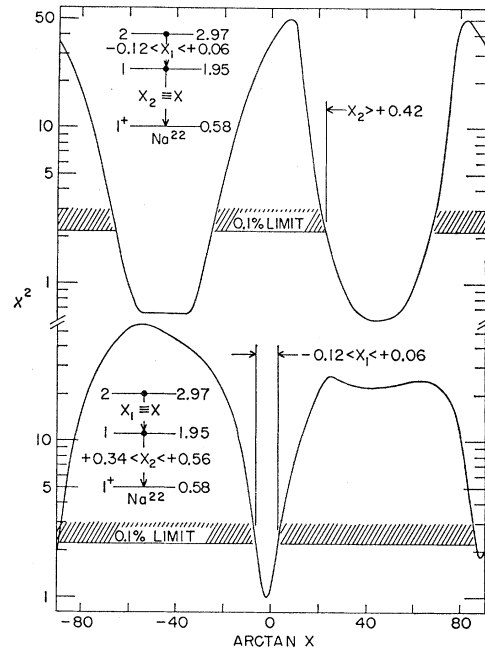


FIG. 10. χ^2 -versus- $\arctan x$ curves for the Na^{22} 2.97 \rightarrow 1.95 \rightarrow 0.58 cascade. The least-squares fit was to the data of Fig. 4 with the spin values are indicated in the level schemes above. For the lower curve x_2 was constrained as indicated (from Table II) and for each value of x_1 the minimum of the envelope of χ^2 is shown for this constraint. The indicated region of x_1 is the only region consistent with the constraints of Table II and with the present fit. In the upper curve x_1 was constrained to the region allowed by the lower curve and for each value of x_2 the minimum of the envelope of χ^2 is shown for this constraint. This curve, together with Table II, results in the constraint $+0.42 < x_2 < +0.56$ for the Na^{22} 1.95 \rightarrow 0.58 transition if the 1.95-MeV level has $J = 1$.

where m takes on all integer values from $-J_1$ to J_1 , J_1 is the spin of the initial level ($J_1=4$ in this case), and $P(-m)=P(m)$ since both the beam and target are unpolarized. Those $P(m)$ values which are identically zero were ones for which a lower value of χ^2 resulted when the $P(m)$ were allowed to be negative. Since this is unphysical, the procedure used was to repeat the fitting procedure with negative values of $P(m)$ constrained at zero.

1.528 \rightarrow 0.891 \rightarrow 0 Cascade

The χ^2 fit to the data of Fig. 7 for the 1.528 \rightarrow 0.891 \rightarrow 0 cascade is displayed in Fig. 9. For this cascade the spin sequence is known¹⁻³ to be $5^+ \rightarrow 4^+ \rightarrow 3^+$ so that this was the only spin combination considered. The display of Fig. 9 shows χ^2 versus $\arctan x_1$ and χ^2 versus $\arctan x_2$. In both cases there is no constraint on the other mixing ratio. It is seen that only one value of x_1 and x_2 give acceptable solutions and thus both are determined by the angular correlation measurement. The phase convention used is that of Litherland and Ferguson⁹ for $E2/M1$ mixtures, which is the same as that recommended by Rose and Brink.¹⁴ The solid curve of Fig. 7 is the fit corresponding to the solutions for x_1 and x_2 of Fig. 9. This solution yielded the following values for the $P(m)$:

$$\begin{aligned} P(0) &= 0.56 \pm 0.47, \\ P(1) &= 0.05 \pm 0.39, \\ P(2) &= 0.07 \pm 0.23, \\ P(3) &= 0.10 \pm 0.07, \\ P(4) &= 0.0, \\ P(5) &= 0.0. \end{aligned}$$

The α energy, 4.9 MeV, was not too much above threshold [$E_{\alpha}(\text{th})=4.21$ MeV] for production of the Na^{22} 1.528-MeV level. Thus $l=0$ neutron emission is expected to dominate the reaction and since $l=0$ neutron emission only populates the $m=0, \pm 1$ substates, the low values of the $P(m)$ for larger values of $|m|$ are consistent with expectations.

It is seen that the $P(m)$ are not accurately determined by this correlation measurement even though x_1 and x_2 are determined quite well. The reason for this is explained in Ref. 9.

2.97 \rightarrow 1.95 \rightarrow 0.58 and 3.06 \rightarrow 1.95 \rightarrow 0.58 Cascades

The analysis of the angular correlation results for these two cascades, Figs. 4 and 5, starts with the information available from previous work,^{1,2} which has restricted the possible spin combinations to those listed in Table II with the spin of the 0.583-MeV level fixed as 1. For each spin combination the mixing ratios of γ_1 and γ_2 are also constrained as indicated in Table II.

¹⁴ H. J. Rose and D. M. Brink, Rev. Mod. Phys. 39, 306 (1967).

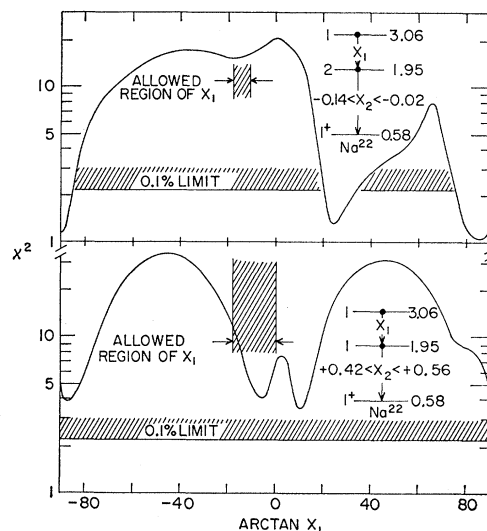


FIG. 11. χ^2 -versus- $\arctan x$ curves for the Na^{22} 3.06 \rightarrow 1.95 \rightarrow 0.58 transition. The lower curve has $J=1$ for the Na^{22} 1.95-MeV level and thus uses the constraint (see Fig. 10) $+0.42 < x_2 < +0.56$ on the 1.95 \rightarrow 0.58 mixing ratio. It is seen that there is no acceptable solution for a $J=1$ assignment to the 3.06-MeV level. Thus, from Table II, we see that the 1.95-MeV level cannot have $J=1$, and has $J=2$. In the upper curve x_2 is constrained according to Table II for a 1-2-1 cascade and it is seen that there is no solution for x_1 within the region allowed by the constraint of Table II. Thus the 3.06-MeV level does not have $J=1$.

We first consider possible fits assuming that the Na^{22} 1.95-MeV level has $J=1$. From Table II we then see that the 2.97-MeV level would have $J=2$ and the 3.06-MeV level would have $J=1$. The appropriate χ^2 plots for the 2.97 \rightarrow 1.95 \rightarrow 0.58 cascade are shown in Fig. 10. The lower plot shows $\arctan x_1$ versus χ^2 with x_2 constrained as indicated in Table II. We see that this fit yields the constraint $-0.12 < x_1 < +0.06$ with our convention of rejecting solutions at the 0.1% limit.¹⁵ This restriction on x_1 , more restrictive than that of Table II, was then used in obtaining the χ^2 -versus- $\arctan x_2$ plot shown in the upper part of Fig. 10. This plot, together with Table II, gives the constraint $+0.42 < x_2 < +0.56$. This constraint was then used in the fit to the 3.06 \rightarrow 1.95 \rightarrow 0.58 correlation shown in the lower part of Fig. 11. Since this latter plot shows no possible solution, the 1.95-MeV level cannot have $J=1$. From Table II we see that it therefore has $J=2$.

The upper part of Fig. 11 illustrates the χ^2 -versus- $\arctan x_1$ plot for the 3.06 \rightarrow 1.95 \rightarrow 0.58 correlation with $J_1=1$, $J_2=2$, and x_2 constrained as indicated in Table II. It is seen that there is no solution in the al-

¹⁵ The 0.1% limit corresponds to ~ 6 standard deviations. Thus it may appear a rather conservative level at which to reject unfavored results and indeed we sometimes reject solutions at the 1% limit. However, in the present experiments, systematic errors are quite important and difficult to assess. We put a great deal of thought and care into their evaluation and do have several checks that they are evaluated fairly accurately. However, the rejection at the 0.1% limit rather than a lower level gives us additional assurance that a correct solution is not being rejected due to a systematic distortion of the data.

lowed range of x_1 (Table II), thus the 3.06-MeV level does not have $J=1$.

A $J=1$ solution for the 2.97-MeV level is ruled out by results shown in Fig. 12. For this plot, with x_1 constrained to the range given in Table II, there is no acceptable solution for any value of x_2 . Thus, from Table II, we see that the 2.97-MeV level must have $J=3$. χ^2 plots for the $2.97 \rightarrow 1.95 \rightarrow 0.58$ correlation with $J_1=3$, $J_2=2$ are shown in Fig. 13. The upper plot, which is for no restriction on x_1 , gives a solution for x_2 consistent with the range $-0.14 < x_2 < +0.14$ of Table II. Combining the result of Fig. 13 with that of Table II gives the 0.1% limit, $-0.035 < x_2 < +0.14$. This constraint was used in the plot shown in the lower part of Fig. 13 which gives the 0.1% limit constraint, $-0.044 < x_1 < +0.07$. To one standard deviation, $x_1 = +(0.017 \pm 0.034)$ and $x_2 = +(0.04 \pm 0.06)$. The solid curve of Fig. 4 shows the best fit to the $2.97 \rightarrow 1.95 \rightarrow 0.58$ correlation for $x_1 = x_2 = 0$.

The upper curve of Fig. 14 illustrates the results of an attempt to fit the $3.06 \rightarrow 1.95 \rightarrow 0.58$ correlation with $J_1=3$, $J_2=2$. The constraint of Table II for x_2 was used and that for x_1 is indicated. It is seen that $J=3$ is not allowed for the 3.06-MeV level which therefore has $J=2$. The lower plot of Fig. 14 illustrates that $J=2$ for the 3.06-MeV level gives an acceptable solution: we find $x_1 = -(0.05 \pm 0.15)$. The solid curve of Fig. 5 is the best fit to the $3.06 \rightarrow 1.95 \rightarrow 0.58$ correlation for $x_1 = x_2 = 0$.

In conclusion we find that the Na^{22} 1.95-MeV level has $J=2$ and the $1.95 \rightarrow 0.58$ transition has a quadrupole/dipole mixing ratio of $+(0.04 \pm 0.06)$. The Na^{22} 2.97- and 3.06-MeV levels have $J=3$ and 2, respectively; while the $2.97 \rightarrow 1.95$ and $3.06 \rightarrow 1.95$ transitions have quadrupole/dipole mixing ratios of $+(0.017 \pm 0.034)$ and $-(0.05 \pm 0.15)$, respectively.

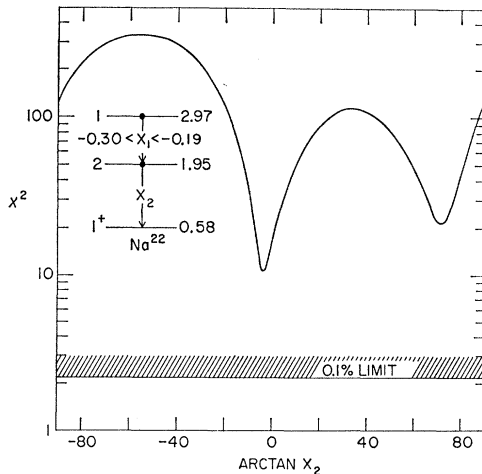


FIG. 12. χ^2 -versus- $\arctan x_2$ for the Na^{22} $2.97 \rightarrow 1.95 \rightarrow 0.58$ cascade. The constraint on x_1 is that of Table II for a 1-2-1 cascade. There is no acceptable solution so the Na^{22} 2.97-MeV level does not have $J=1$. From Table II, then, it must have $J=3$.

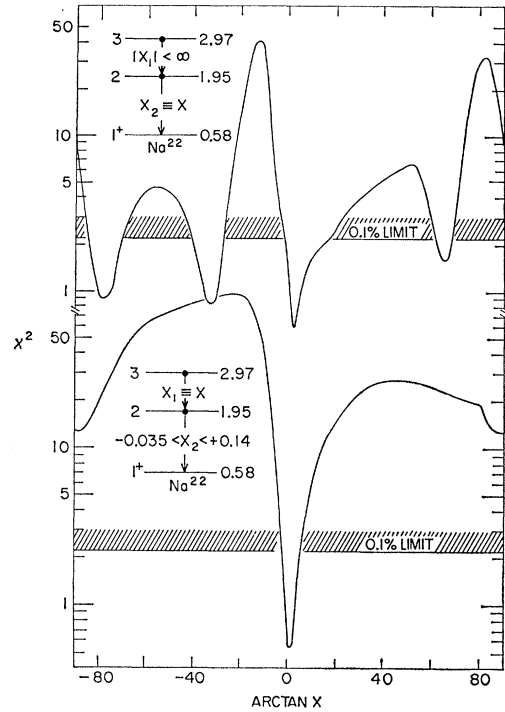


FIG. 13. χ^2 -versus- $\arctan x$ curves for the Na^{22} $2.97 \rightarrow 1.95 \rightarrow 0.58$ cascade with the spin values as shown in the level schemes. In the upper curve there is no restriction on x_1 . The curve gives the constraint on x_2 used in the lower curve which in turn gives the following constraint on x_1 : $-0.044 < x_1 < +0.07$. These constraints on x_1 and x_2 are consistent with those of Table II; thus $J=3$ for the Na^{22} 2.97-MeV level gives an acceptable solution.

IV. DISCUSSION

A. Synthesis with Previous Data

As indicated in Fig. 1, we identify¹ the Na^{22} 1.95-MeV level as the $J^\pi=2^+$, $T=1$ analog of the first-excited state of Ne^{22} . Experimentally, however, the parity of the 1.95-MeV level has not yet been determined. The 0.583-, 2.97-, and 3.06-MeV levels have all been assigned $T=0$;¹ thus the γ -ray transitions connecting these three states with the 1.95-MeV level are all $\Delta T=1$ and so are expected¹ to be predominantly dipole. This is in agreement with the values we have found for their quadrupole/dipole mixing ratios—all three being consistent with pure dipole radiation.

There have been three measurements reported of the mean lifetime of the Na^{22} 1.528-MeV level, 3.8 ± 0.9 psec,¹ $3.9_{-1.0}^{+2.2}$ psec,⁵ and 3.2 ± 1.0 psec.⁷ These are in good agreement and we adopt the average 3.6 ± 0.75 psec. For the Na^{22} 0.891-MeV level, Doppler-shift measurements have yielded > 8 psec,¹ $11.1_{-3.7}^{+11.2}$ psec,⁵ 11.4 ± 1.8 psec,⁶ and 18 ± 7 psec.⁷ Again, these are in good agreement and we adopt 12 ± 1.8 psec.

For the mixing ratio of the Na^{22} $0.891 \rightarrow 0$ transition we adopt the average $-(3.19 \pm 0.26)$ of the present work with two earlier measurements $-(3.0 \pm 0.6)$ ¹ and

TABLE III. Results for the electromagnetic decay of the Na^{22} 1.528- and 0.891-MeV levels.

Transition (MeV)	τ (partial) (psec)	$x(E2/M1)$	Transition strength (Weisskopf units)
			$E2$ $M1$
1.528 \rightarrow 0	3.8 ± 0.75	...	$6.9_{-1.2}^{+2.0}$...
1.528 \rightarrow 0.891	80.0 ± 27.0	$-(2.00 \pm 0.15)$	20.7 ± 7.0 $(3.0 \pm 1.1) \times 10^{-4}$
0.891 \rightarrow 0	12.0 ± 1.8	$-(3.19 \pm 0.26)$	29.5 ± 5.0 $(3.3 \pm 0.6) \times 10^{-4}$

$-(3.6 \pm 0.6)$.^{5,16} For the 1.528 \rightarrow 0.891 transition there is only the present measurement, $x = -(2.00 \pm 0.15)$. The available information on the branching ratios of the Na^{22} 1.528- and 0.891-MeV levels is listed in Table I.

The $M1$ and $E2$ transition strengths of the three transitions connecting the Na^{22} 0.0-, 0.891-, and 1.528-MeV levels are listed in Table III. The transition strengths are in Weisskopf units.¹⁷

B. Rotational-Model Description of Na^{22}

We now shall compare the known properties of the low-lying states of Na^{22} , including the results of Table III, with the predictions of the rotational model.

For Na^{22} the rotational model predicts that the intrinsic spin projections along the nuclear symmetry axis of protons and neutrons are $\Omega_p = \Omega_n = \frac{3}{2}$.¹⁸ Thus, three low-lying rotational bands are predicted¹⁸⁻²¹: one with $K = \Omega_p + \Omega_n = 3$ having $T=0$ and a 3^+ , 4^+ , 5^+ ... spin sequence and two with $K = \Omega_p - \Omega_n = 0$. For $K=0$, there exist antisymmetric and symmetric combinations of the wave functions for Ω_p and Ω_n . The first combination has $T=1$ and a 0^+ , 2^+ , 4^+ ... spin sequence, while the second has $T=0$ and a 1^+ , 3^+ , 5^+ ... spin sequence. In odd-odd nuclei the residual interaction is found to separate the intrinsic energies of the $K = \Omega_p + \Omega_n$ states from the $K = \Omega_p - \Omega_n$ states, with the former appearing at a lower energy.²¹ No simple prediction can be made for the relative binding energies of the intrinsic states of the $T=0$ and $T=1$, $K=0$ bands.²¹ Our identification of the members of these three bands is illustrated in Fig. 15 where the excitation energies of these states are plotted against $J(J+1)$. We have identified the Na^{22} 0.0-, 0.891-, and 1.528-MeV levels as the 3^+ , 4^+ , 5^+ levels of the $K=3$ band and have included our speculation¹⁻³ that the 3.71-MeV level is the 6^+ member of this band.

¹⁶ Because it is in disagreement with the three quoted measurements, we exclude from this average the value $x(E2/M1) = -(1.7 \pm 0.9)$ extracted from the work of Carola [G. T. Carola, M.S. thesis, University of Alberta, Edmonton, Canada, 1965 (unpublished)] by J. G. Pronko [H. J. Maier, D. Pelte, J. G. Pronko, and C. Rolfs, Nucl. Phys. 84, 1 (1966)].

¹⁷ D. H. Wilkinson, in *Nuclear Spectroscopy*, edited by F. Ajzenberg-Selove (Academic Press Inc., New York, 1960), Part B, p. 862 ff.

¹⁸ A. Bohr and B. R. Mottelson, Kgl. Danske Videnskab. Selskab, Mat.-Fys. Medd. 27, No. 16 (1953); S. G. Nilsson, *ibid.* 29, No. 16 (1955).

¹⁹ G. Rakavy, Nucl. Phys. 4, 375 (1957).

²⁰ G. M. Temmer and N. P. Heydenburg, Phys. Rev. 111, 1303 (1958).

²¹ O. Nathan and S. G. Nilsson, in *Alpha-, Beta-, and Gamma-Ray Spectroscopy*, edited by K. Siegbahn (North-Holland Publishing Co., Amsterdam, 1965), Vol. I, p. 597.

We note that the 3.71-MeV level is the *lowest* energy level of Na^{22} which could conceivably be this 6^+ state. The 0.583- and 1.984-MeV levels are identified as the 1^+ and 3^+ members of the $J=0$, $T=0$ band, although the spin of the latter state has not been determined. The 3.53-MeV level is the lowest Na^{22} state which could be the 5^+ member of this band; its identification, however, is highly speculative. The $K=0$, $T=1$ band shown in Fig. 15 is actually that of Ne^{22} (see Ref. 12) with the excitation energy of the Na^{22} 0^+ , $T=1$ 0.657-MeV level added to that of each Ne^{22} state. The identification of the 2^+ and 4^+ members of this band in Na^{22} can be inferred from Fig. 1.

It can be seen from Fig. 15 that the well-known rule for the energy levels of a nearly rigid rotator,²¹

$$J_J = A_1 J(J+1) + A_2 [J(J+1)]^2, \quad (1)$$

with $|A_2| \ll |A_1|$, is only approximately obeyed, so that

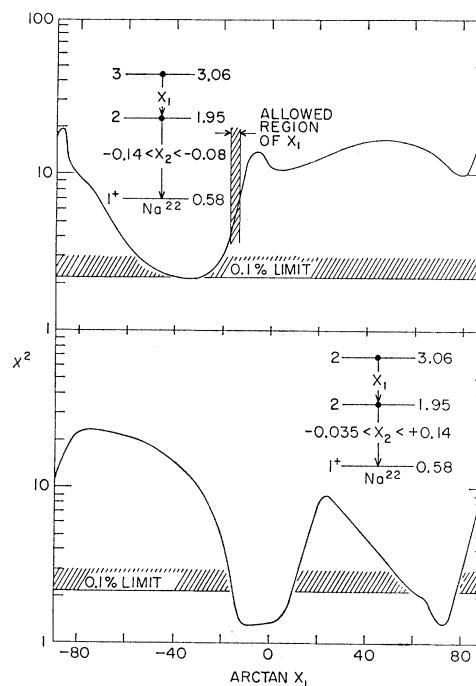


FIG. 14. χ^2 -versus- $\arctan x$ curves for the Na^{22} 3.06 \rightarrow 1.95 \rightarrow 0.58 cascade with the spin values as given in the level schemes. In the upper curve x_2 was constrained as given in Table II and there is no acceptable solution for x_1 within the range allowed by the constraint of Table II. Thus the 3.06-MeV level cannot have $J=3$ and from Table II we see it has $J=2$. In the lower curve $J=2$ for the 3.06-MeV level and x_2 is constrained as determined from the results of Fig. 13. The 2-2-1 curve shows an acceptable solution and gives $x_1 = -(0.05 \pm 0.15)$.

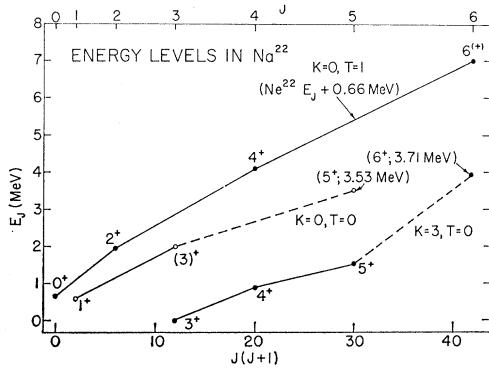


FIG. 15. Level sequences for the three lowest rotational bands of Na^{22} compared to the expected dependence of $J(J+1)$. Speculative assignments, denoted by dashed lines and parentheses, are discussed in the text.

there are some rather strong perturbations if, in actual fact, these three rotational bands do exist at all. We now shall consider the diagonal and off-diagonal $E2$ and $M1$ matrix elements connecting the states of these three bands. We shall see that they are consistent with the rotational model which therefore must be given some credence. We first consider the $E2$ transitions connecting levels of the same band.

The first-order prediction for intraband $E2$ transition strengths is (in units of barns²)

$$B(E2) = (5/16\pi) Q_0^2 (J_i 2K0 | J_f K)^2 e^2. \quad (2)$$

$B(E2)$ is related to $|M(E2)|^2$, given in Weisskopf units, by

$$B(E2) = 5.94 \times 10^{-6} A^{4/3} |M(E2)|^2 e^2, \quad (3)$$

where A is the atomic number. In Eq. (2), $(J_i 2K0 | J_f K)$ is a Clebsch-Gordan coefficient and Q_0 is the intrinsic quadrupole moment of the rotating system measured in barns. We give, in Table IV, the values of Q_0 extracted from measured transition strengths using Eqs. (2) and (3). The $|M(E2)|^2$ for the $K=3$ band are given in Table III. The $K=0$, $T=1$ results^{13,22} are for Ne^{22} , while that for $K=0$, $T=0$ is from Ref. 1. We see from

TABLE IV. Intrinsic quadrupole moments for the known intraband $E2$ transitions of mass 22 extracted from measured values of $B(E2)$.

Transition	J_i, J_f	K, T	$10^4 B(E2)$ ($e^2 \text{ b}^2$)	Q_0 (b)
$\text{Na}^{22} 0.891 \rightarrow 0$	4, 3	3, 0	108 ± 18	$+0.56 \pm 0.05$
$\text{Na}^{22} 1.528 \rightarrow 0.891$	5, 4	3, 0	76 ± 26	$+0.48 \pm 0.08$
$\text{Na}^{22} 1.528 \rightarrow 0$	5, 3	3, 0	$25.3_{-4.4}^{+7.3}$	$+0.55 \pm 0.06$
$Q_0(3,0) = +0.54 \pm 0.04^a$				
$\text{Na}^{22} 1.984 \rightarrow 0.583$	3, 1	0, 0	93_{-16}^{+25}	$+0.60 \pm 0.06$
$Q_0(0,0) = +0.60 \pm 0.06^a$				
$\text{Ne}^{22} 1.275 \rightarrow 0$	2, 0	0, 1	43 ± 9	$+0.46 \pm 0.05$
$\text{Ne}^{22} 3.375 \rightarrow 1.275$	4, 2	0, 1	54_{-9}^{+14}	$+0.44 \pm 0.05$
$Q_0(0,1) = +0.50 \pm 0.05^{a,b}$				

^a $Q_0(K,T)$ is the average Q_0 for a given K, T .

^b $Q_0(0,1)$ is increased by 10% since the $B(E2)$ are for Ne^{22} and the rotational model predicts that Q_0 is proportional to Z (see Ref. 18).

²² S. J. Skorka, J. Hertel, and T. W. Retz-Schmidt, Nucl. Data 2, 347 (1967).

Table IV that the Q_0 for a given band are consistent with each other; therefore the relative $E2$ transition strengths for a given K, T obey the prediction of Eq. (2). Furthermore, the $Q_0(K,T)$, i.e., the average Q_0 for a given band, are observed to be roughly the same for each of these three bands. There is at best only slight evidence for a dependence of Q_0 on K, T ; the relative Q_0 are in the ratio $Q_0(0,1):Q_0(3,0):Q_0(0,0) = 1:(1.08 \pm 0.13):(1.20 \pm 0.17)$. This possible dependence is not inconsistent with that expected from the difference in the moments of inertia of the three bands.¹⁸ However, these moments of inertia are given by the slopes of the E_J -versus- $J(J+1)$ curves of Fig. 15 and it is clear from this figure that they are only roughly determined.

We have taken the positive sign for Q_0 in Table IV because local systematics indicate a prolate deformation for Na^{22} . For instance, the measured quadrupole moments of the $N=11$ and $Z=11$ ground states of Ne^{21} and Na^{23} are $+(0.093 \pm 0.010)$ and $+(0.10 \pm 0.011)$ b, respectively.^{23,24} Incidentally, these electric quadrupole moments correspond to values for Q_0 of $+(0.47 \pm 0.05)$ and $+(0.51 \pm 0.06)$, respectively.¹⁸ These are, as expected, close to the Q_0 for Na^{22} .

We now consider the intraband $M1$ matrix elements of Na^{22} . The $M1$ transition strength for an $I+1 \rightarrow I$ transition in a rotational band with K odd is¹⁸

$$|M(M1)|^2 = B(M1)/B(M1)_{sp} = 0.1333(g_K - g_R)^2 K^2 (J_i 1 K 0 | J_f K)^2 \quad (4)$$

in terms of the gyromagnetic ratios of the intrinsic and collective motion, g_K and g_R . We can use Eq. (4) to extract values of $|g_K - g_R|$ from the $M1$ strengths of the $5^+ \rightarrow 4^+$ 1.528 \rightarrow 0.891 and $4^+ \rightarrow 3^+$ 0.891 \rightarrow 0 transitions in Na^{22} . The results, using Table III, are 0.029 ± 0.005 and 0.038 ± 0.004 , respectively. Since these two values of $g_K - g_R$ just overlap, the relative $M1$ strengths are consistent with the prediction of the strong-coupling rotational model. We adopt $|g_K - g_R| = 0.034 \pm 0.004$ for purposes of discussion.

The static magnetic moment μ of a state in a rotational band ($K \neq \frac{1}{2}$) may be expressed as,

$$\mu = [K^2/(J+1)](g_K - g_R) + Jg_R. \quad (5)$$

The ground-state magnetic moment of Na^{22} has been measured²⁵ to be $+(1.746 \pm 0.003)$ nuclear magnetons while measurements for that of the 1^+ 0.583-MeV level yield $+(0.535 \pm 0.010)$ nuclear magnetons¹¹ and $+(0.555 \pm 0.017)$ nuclear magnetons.²⁶ [We adopt the weighted average of these latter two measurements,

²³ G. M. Grosf, P. Buck, W. Lichten, and I. I. Rabi, Phys. Rev. Letters 1, 214 (1958).

²⁴ M. L. Perl, I. I. Rabi, and B. Senitzky, Phys. Rev. 98, 611 (1955).

²⁵ L. Davis, Jr., D. E. Nagle, and J. R. Zacharias, Phys. Rev. 76, 1068 (1949).

²⁶ H. Schmidt, J. Morgenstern, H. J. Körner, J. Braunsfurth, and S. J. Skorka, Phys. Letters 24B, 457 (1967).

$+(0.540 \pm 0.009)$ nuclear magnetons, for purposes of discussion.] From Eq. (5) we see that the magnetic moment of the 1^+ 0.583-MeV level is just g_R , which is predicted to be independent of K, T .¹⁸ From the measured magnetic moments for the ground state and first excited state and Eq. (5), we obtain

$$\begin{aligned} g_R &= +(0.540 \pm 0.009), \\ g_K &= +(0.596 \pm 0.003), \\ g_K - g_R &= +(0.056 \pm 0.012). \end{aligned}$$

The value extracted for g_K is in excellent agreement with that calculated for the Na^{22} ground state by Bohr and Mottleson,¹⁸ while g_R is consistent with the prediction $g_R \sim Z/A$.¹⁸ The magnitude of $g_K - g_R$ extracted from the magnetic moments does not quite overlap with that obtained from the $M1$ transition strength, $|g_K - g_R| = 0.034 \pm 0.004$: nevertheless, considering the approximations inherent in this analysis, the agreement is considered to be quite satisfactory.

Finally we compare the signs of the $E2/M1$ mixing ratios to the predictions of the rotational model. The prediction is²¹

$$\text{sgn}[x(E2/M1)] = -\text{sgn}[(g_K - g_R)/Q_0], \quad (6)$$

where the sign convention is that of Rose and Brink.¹⁴ Since the rotational model predicts both Q_0 and $g_K - g_R$ to be positive it also predicts from Eq. (6) that the $1.528 \rightarrow 0.891$ and $0.891 \rightarrow 0$ transitions have negative values of $x(E2/M1)$, in agreement with experiment (Table III).

Further evidence in support for a rotational-model interpretation of the low-lying states is provided by the apparent effectiveness of ΔK selection rules. The very high $\log ft$ ($=7.6$) for the β decay of the 3^+ Na^{22} ground state ($K=3$) to the 2^+ Ne^{22} first excited state ($K=0$) has been noted previously^{19,27} as has the very small strength, 0.0092 ± 0.0008 W.u.,¹¹ for the $E2$ decay of the 1^+ 0.583-MeV level ($K=0$) to the 3^+ ground state

($K=3$). In addition, the 1.984-MeV level, presumed to be the 3^+ member of the $K, T=0, 0$ band, does not decay to any member of the $K=3$ rotational band with any appreciable strength; in particular, the $1.984 \rightarrow 0$ $E2$ strength is less than 0.06 W.u.¹

We have included in Fig. 15 our speculation that the 3.53- and 3.71-MeV levels of Na^{22} are the 5^+ and 6^+ members of the $K, T=0, 0$ and $3, 0$ bands, respectively. This speculation is based on the restrictions (see Fig. 1) of $J \geq 2$ for these two levels and on their decay modes.² The 5^+ level is predicted to decay 100% to the 3^+ , $K, T=0, 0$ level which we assume to be that at 1.984 MeV. In actual fact the 3.53-MeV level probably decays mainly to this level (transitions to the 1.95-, 1.98-, and 2.21-MeV levels were unresolved)² but has other decay modes, in particular, a $(14 \pm 6)\%$ branch to the ground state and a possible $(13 \pm 5)\%$ branch to the 4^+ 0.891-MeV level.² These latter two branches would be ΔK forbidden if the 3.53-MeV level is the 5^+ state of $K, T=0, 0$.

The 3.71-MeV level decays to the 4^+ 0.891-MeV level and the 5^+ 1.528-MeV level with branching ratios of (65 ± 10) and $(35 \pm 10)\%$, respectively. These are in excellent agreement with the predicted branching ratios of 66 and 34% obtained using $Q_0=0.54$ and $g_K - g_R = +0.034$. With these latter values the mean lifetime of the 3.71-MeV level is predicted to be 0.07 ± 0.01 psec while the mixing ratio for the $3.71 \rightarrow 1.53$ decay is expected to be $x = -(5.6 \pm 1.5)$, i.e., almost pure quadrupole.

Higher rotational bands with either or both Ω_p and Ω_n not equal to $\frac{3}{2}$ are possible for Na^{22} . The 1^+ 1.937-MeV level and 1^- 2.221-MeV level could conceivably be the intrinsic states of such bands. However, it is not fruitful to speculate about these other bands or about higher states of the bands considered here until more experimental work has been done on the Na^{22} states above 2.5-MeV excitation.

ACKNOWLEDGMENT

We would like to thank S. Kahana for discussions concerning the rotational-model interpretation of Na^{22} .

²⁷ The upper limit of 2% (Table I) on the branching ratio of the Na^{22} $1.952 \rightarrow 0$ transition is consistent with this high $\log ft$ value. See D. Kurath, Argonne National Laboratory Report No. ANL-7108, 1965 (unpublished).